


Experimental determination of shock speed versus exciter speed in a two-dimensional dusty plasma

Anton Kananovich  and J. Goree

Department of Physics and Astronomy, University of Iowa, Iowa City, Iowa 52242, USA



(Received 9 May 2019; revised manuscript received 24 July 2019; accepted 16 March 2020; published 28 April 2020)

A shock that is continuously driven by a moving exciter will propagate at a speed that depends on the exciter speed. We obtained this dependence experimentally, in a strongly coupled dusty plasma that was prepared as a single two-dimensional layer of charged microparticles. Attaining this result required an experimental advance, developing a method of driving a shock continuously, which we did using an exciter moving at a constant supersonic speed, analogous to a piston in a cylinder. The resulting compressional pulse was a shock that propagated steadily without weakening, ahead of the moving exciter. We compare our experimental results to an empirical form $M_{\text{shock}} = 1 + sM_{\text{exciter}}$, and to the prediction of a recent simulation.

DOI: [10.1103/PhysRevE.101.043211](https://doi.org/10.1103/PhysRevE.101.043211)

I. INTRODUCTION

Shock waves are strongly nonlinear pulses that propagate at a supersonic speed. Shocks can be generated either impulsively or continuously, according to whether the energy input is, respectively, momentary (e.g., an explosion) or sustained (e.g., a moving piston). Many kinds of substances can support shocks, including obviously gases [1,2], as well as solids [3] and plasmas [4]. Shocks generally have a spatial feature with a large gradient, which is often modeled theoretically as a discontinuity, and this feature moves through the medium at a supersonic speed, with a speed v_{shock} .

There is a traditional empirical relationship between the shock speed v_{shock} and the speed of the particles (i.e., molecules) $v_{\text{particles}}$ in the substance just behind the moving shock. This expression is linear

$$v_{\text{shock}} = a + s v_{\text{particles}}. \quad (1)$$

Historically, the use of Eq. (1) dates back to sometime before 1963, when Alder [5] mentioned that it had been experimentally observed in many substances. A theoretical justification for Eq. (1) was presented in 1967 by Ruoff, using a derivation that included a series expansion [6]. Ruoff also listed some of the substances in which this expression had previously been observed experimentally, and these included pure metals, alloys, ionic solids, covalent solids, and various liquids [6]. The usefulness of this expression was extended later to also include shocks in water [7].

For continuously driven shock waves, produced by an exciter moving at a steady speed v_{exciter} , Eq. (1) can be shown (see Ref. [8] for Supplemental Material) to be equivalent to

$$M_{\text{shock}} = 1 + s M_{\text{exciter}}. \quad (2)$$

Here,

$$M_{\text{shock}} \equiv v_{\text{shock}}/c_l$$

and

$$M_{\text{exciter}} \equiv v_{\text{exciter}}/c_l,$$

where c_l is the longitudinal sound speed.

In this paper, we present experimental results for a continuously driven shock wave in a two-dimensional (2D) dusty plasma, which was made possible by using a new kind of moving exciter. We compare the linear relationship, Eq. (2), with the experimental data. We also compare our results with those of a recent simulation [9]. We will next explain the type of plasma what we use in our experiment.

Plasmas are, generally speaking, comprised of multiple charged species, which can be weakly or strongly coupled. Weakly coupled plasma species have a random kinetic energy that greatly exceeds the interparticle Coulomb potential energy, which is to say that they are not dominated by Coulomb collisions. Strongly coupled species have the opposite condition; their Coulomb interparticle potential energy exceeds the thermal energy so that neighboring particles influence one another greatly. Strong coupling leads to solid or liquid-like behavior, unlike the gas-like behavior that is typical under weak coupling. Due to their low mass, electrons are usually weakly coupled, but heavier charged species can be strongly coupled, as in laser-cooled non-neutral plasmas [10], interiors of giant planets or white dwarfs [11,12], and the warm dense matter generated by intense laser pulses applied to solid surfaces [13–15]. All of these plasmas can sustain shocks.

Dusty plasma is another kind of plasma that can sustain a shock [16–46]. Sometimes called complex plasma or fine-particle plasma, a dusty plasma is comprised of electrons, ions, neutral gas molecules, and solid particles of microscopic size [47–53]. By collecting electrons and ions, these solid microparticles gain large electric charges and thereby become strongly coupled [11,49,51,52,54]. This strong coupling allows dusty plasma experimenting to serve as a tabletop approach for disentangling effects that complicate strong coupling in warm dense matter [55]. In a dusty plasma, the strong coupling can reach such great levels that the particles self-organize into a solid or liquid-like structure [56–68]. The large charge of the microparticles also allows the experimenter to levitate them, against the downward force of gravity, by using an electric force, which is strongest near the boundary of

the plasma, at the sheath edge. By configuring the confining forces, so that the confinement is strong in the vertical direction and weak in the horizontal direction, we are able to levitate a single layer of microparticles, so that we have prepared a 2D dusty plasma.

Shocks have been observed in dusty plasma experiments having a compressional pulse propagating at a supersonic velocity ($M_{\text{shock}} > 1$) relative to the microparticle cloud as a whole. The relevant sound speed for the supersonic condition is the one for longitudinal motion of the microparticle species, which is typically $c_l \approx 2$ cm/s. Such shock experiments have been performed for several plasma configurations, with the ionization sustained by either dc [20,21,25,27,28,69] or rf [16,17,19,23,24] power, and microparticle clouds that filled either a three-dimensional (3D) volume [18,20–22,25–30,69] or a 2D monolayer [16,17,19,24].

Previous experiments with shocks in 2D dusty plasma involved Mach cones [16,17,23,24] and blast waves [19]. A Mach cone is created by a supersonic moving disturbance analogous to an airplane, while a blast wave results from a localized impulsive event, like an explosion. Blast wave experiments were performed by Samsonov *et al.*, who relied on a pulsed voltage applied to a wire which was not moving, but was stationary [19]. The resulting compressional pulse had a speed exceeding the microparticles sound speed, with a Mach number as high as $M_{\text{shock}} = 2.7$. This supersonic speed for the pulse, along with a sharp gradient (jump) in a hydrodynamic parameter, allowed Samsonov *et al.* to identify their blast-wave pulse as a shock. Due to the impulsive generation method, these blast waves had an amplitude that was highest at the beginning of the propagation, gradually becoming weaker closer to the end [19].

Our experimental goal, to measure the dependence of shock speed on the exciter's speed, requires not a blast wave, but a continuously driven shock, one that is sustained by an exciter moving at a steady and controllable speed. This is analogous to an exciter piston moving steadily at a supersonic speed in a cylinder of gas, which is a common textbook topic [1,70].

Previous experimenters achieved continuously driven shock waves in dusty plasmas that are 3D, i.e., with more than one layer. The microparticle cloud moved past a stationary obstacle due to an external force, provided either by a neutral gas pressure gradient [28,30] or by tilting the lower electrode [29]. Such schemes have been demonstrated to drive a useful shock wave in a 3D microparticle cloud, but not yet in a 2D cloud.

Generating a continuously driven shock wave in a 2D cloud is made possible for our experiment by an instrumentation advance: the development of a method of driving a shock continuously. Previous experiments with shocks in 2D dusty plasmas did not use an exciter that was moving, as ours does, at a steady and controllable speed.

Our advance in the experimental method was made possible by using, as a moving exciter, a wire that was propelled mechanically. The wire itself was similar to that of Samsonov *et al.*, but ours was not stationary. It was mounted on a motorized probe drive capable of sustaining a steady speed, which was supersonic as compared to the sound wave in the dust component.

II. RECENT SIMULATIONS

Our experiment is motivated by recent simulations, which all used a charged exciter moving at a steady supersonic speed to excite a shock in a 2D dusty plasma. A series of three simulation papers began with Tiwari and Sen [71] and Marciante and Murillo [72]. The latter authors identified a need for dusty plasma experiments with a continuously driven shock, analogous to a piston-driven shock in a gas cylinder, and they noted that such an experiment would open the door to close comparison with simulations [72]. This need is fulfilled by the experiment we report here.

The most recent simulation, by Lin *et al.* [9] had, as a major result, a graph of the shock speed's dependence on the mean particle speed measured at a location after the shock. The authors of [9] prepared such graphs for a range of parameters spanning liquid-like and solid-like conditions. They fit their simulation results to an empirical form:

$$D = C_0 + B\bar{v} + A\bar{v}^2, \quad (3)$$

where C_0 , B , and A are fit coefficients, and D and \bar{v} are shock speed and the mean particle speed behind the shock, both normalized by the product of Wigner-Seitz radius and nominal plasma frequency $a\omega_{\text{pd}}$. Physically, Eq. (3) is essentially a generalization of Eq. (1) by adding a quadratic term, although the authors of [9] did not mention this.

In this paper we seek to compare our experimental results not only to the traditional empirical relationship of Eq. (2), but also the recent suggestion of Eq. (3). However, we need to express Eq. (3) in another form, in terms of our observables M_{shock} and M_{exciter} . To do so, we make two substitutions. First, we replace the particle speed \bar{v} behind the shock with the exciter speed. The suitability of this substitution was confirmed by the simulation of [9] for a 2D dusty plasma, as well as standard textbooks for other substances [2,70]. Second, the coefficient C_0 in Eq. (3) was explained by Lin *et al.* to correspond to the physical sound speed, expressed in units of $a\omega_{\text{pd}}$ [9]. For this reason, we can replace \bar{v} with $C_0 M_{\text{exciter}}$, and we replace D with $C_0 M_{\text{shock}}$. After these two substitutions, Eq. (3) takes the form suitable for comparison with our experiment

$$M_{\text{shock}} = 1 + BM_{\text{exciter}} + AC_0 M_{\text{exciter}}^2. \quad (4)$$

III. EXPERIMENT

A. Dusty plasma preparation

Argon gas at a steady pressure of 1.8 Pa was partially ionized by radiofrequency (rf) power at 13.5 MHz applied to a horizontal lower electrode. The other electrode was the grounded vacuum chamber. The rf peak-to-peak voltage was constant at 184 V. Using capacitive coupling, a dc self bias of -85.5 V developed on the lower electrode.

Spherical melamine-formaldehyde microparticles were dispensed from a shaker located above the plasma. As they fell, the microparticles acquired a negative electric charge, allowing them to settle in a single horizontal layer at a stable height a few mm above the lower electrode, where an upward electric force balanced downward gravity, as schematically shown in Fig. 1. In this respect we made a 2D dusty plasma, where the microparticles occupied a 2D layer immersed in a

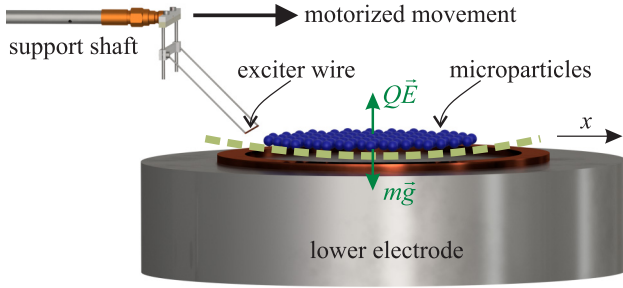


FIG. 1. Experimental setup. A horizontal exciter wire was moved in the positive x direction. Its support structure is drawn to scale, while other features are only sketched schematically. A 2D layer of microparticles was levitated in the upper part of the sheath, sketched as a dashed line, above the powered rf electrode in a vacuum chamber. The sheath had a gentle bowl shape, due to a combination of a strong vertical electric field and a weaker horizontal component, which confined microparticles laterally. The Supplemental Material [8] includes photographs of the chamber, top-view camera, and optics for illuminating the microparticles.

partially ionized argon plasma, which filled the chamber. The microparticles were monodisperse, with a $8.69 \mu\text{m}$ diameter, and a $5.2 \times 10^{-13} \text{ kg}$ mass. They experienced gas drag force with a coefficient (force divided by momentum) that we calculated as 2.4 s^{-1} , for our gas pressure.

We verified that the cloud of microparticles formed a single horizontal layer by imaging it by a side-view camera. One advantage of a single layer is its tendency to form a stable 2D crystalline lattice, which was triangular with six-fold symmetry, i.e., hexagonal. Images of this crystalline lattice are shown in the Supplemental Material [8].

B. Measurement method

In order to measure the parameters of the microparticle cloud and the propagating pulse, we imaged the microparticles directly, using video microscopy [73–75]. This was possible because micron-sized particles scatter light so that they were easily seen, and they moved slowly, typically $\ll 1 \text{ m/s}$. We obtained spatiotemporal measurements not only of the entire particle cloud, but also the positions and velocities of individual microparticles [73–76]. Measurements of this kind have been used by many experimenters [58,77–82]. This approach is especially well suited for 2D dusty plasmas, where the microparticles all lie in a single plane, so that they all can be imaged.

To allow video microscopy, the cloud of microparticles was illuminated by a 532-nm continuous-wave laser. This illumination beam was shaped into a horizontal sheet with a vertical thickness of 1 mm, which was sufficient to avoid the previously reported problem of microparticles vanishing from view during a shock’s propagation [19].

A high-speed camera imaged the microparticle cloud from above. We used a 12-bit monochrome Phantom Miro M120 with a 105-mm macro lens and a bandpass filter. The camera’s field of view (FOV) was $41 \times 31 \text{ mm}$, including ≈ 2000 microparticles in the early portion of a shock’s propagation. (A cloud size of a few thousand microparticles was previously

shown experimentally [19] and in a simulation [72] to be large enough to sustain a shock wave.) The FOV’s lower-left corner defines the origin of our x - y coordinate system. The camera recorded at 870 frames/s, with an exposure time (acquisition time) of $1000 \mu\text{s}$ per image, which was short enough that moving microparticles never appeared elongated in our shocks. Further apparatus details are in the Supplemental Material [8].

Particle tracking velocimetry analysis yielded the positions and velocities of microparticles in each video frame. Positions, which were our primary measurement, were obtained with subpixel accuracy using the moment method [73,83]. Additionally, we obtained velocities of microparticles by tracking them for two consecutive frames [74,75].

C. Microparticle cloud parameters

We used our measurements to obtain microparticle cloud parameters in the undisturbed crystalline equilibrium state, as we describe below. These measurements were all obtained by analyzing videos of the crystalline state, at the beginning and end of the experiment.

Still images, from individual frames in the crystalline state, were analyzed to yield the undisturbed areal density as $n = 1.81 \text{ mm}^{-2}$. This was obtained simply by counting microparticles. The corresponding two-dimensional Wigner-Seitz radius was $a = 0.42 \text{ mm}$, and the lattice constant for the triangular lattice was $b = 0.80 \text{ mm}$.

Particle motion, in the sequence of frames in the crystalline state, provided six more parameters, for the undisturbed cloud. The root-mean-square velocity of the microparticles was $v_{\text{rms}} = 0.499 \text{ mm/s}$. By fitting theoretical dispersion relations to our experimental dispersion relations, we obtained the screening parameter $\kappa = 1.6$ and the nominal 2D plasma frequency $\omega_{\text{pd}} = 49 \text{ s}^{-1}$. These parameters allowed us to calculate the charge $Q/e = -1.4 \times 10^4$ and Coulomb coupling parameter $\Gamma = 1.7 \times 10^3$.

The longitudinal sound speed, which of course is important in characterizing shocks, was found to be $c_l = 19 \text{ mm/s}$. This value was obtained by an input of experimental parameters listed above, into a theoretical graph [84] of sound speed. The underlying theory is based on a dispersion relation for a 2D triangular lattice with a Yukawa interaction, which is also the case for the dispersion relation analysis mentioned above.

Numerical values for the parameters listed above were obtained as the average of two measurements, at the beginning and end of the experiment. In each case, the measurement was for the crystalline equilibrium state. Further details of these measurements are described in the Supplemental Material [8], where we also define the parameters a , ω_{pd} , κ , Γ .

D. Manipulation method

The primary difference between our experimental setup and that of Samsonov *et al.* [19] was our manipulation scheme, which allowed us to obtain a compressional pulse with a different character. The manipulation in [19] was impulsive (it relied on an electrical pulse applied to a stationary wire), and the resulting pulse is therefore classified as a *blast*

wave [72]. We used instead a steadily moving exciter, so that our shock was *continuously driven* at a controlled speed. This approach allowed us to obtain the dependence of the pulse speed on the speed of the moving exciter.

Our compressional pulses in the microparticle cloud were generated by electrical repulsion from an exciter wire, moved at a steady speed. The 0.41-mm diameter wire was oriented horizontally several mm above the plane of the microparticles. Electrically, the wire was floating at a natural potential due to steady collection of electrons and ions. Microparticles, which were also electrically floating, were repelled by the wire because they had the same polarity. Initially, the wire was at rest at $x = -60$ mm, far to the left of the particle cloud. The wire was then moved in the $+x$ direction at a constant speed. To achieve a supersonic speed for the exciter wire, we used a stepper motor with a torque as high as 0.7 Nm to drive a linear translation stage, outside the vacuum chamber, pushing the wire's support shaft deeper into the chamber [8].

E. Experimental runs

The experiment was carried out with videos recorded for six runs with manipulation by the moving wire. Between these manipulation runs, we allowed about 20 min for the cloud to relax to its original position and to anneal into a crystalline microstructure. At the beginning and end of the experiment, we recorded videos of the particle motion in the crystalline equilibrium state, to allow us to characterize the microparticle cloud parameters including charge, undisturbed areal density, screening length, and other parameters, as described in Sec. III C above. These parameters describe the conditions of microparticles exactly where they were located, within the upper portion of the sheath, because they are based on measurements of the microparticles themselves; these parameters do not reflect conditions elsewhere in the plasma. Before all of these videos were recorded, which required five hours, it was necessary to prepare a cloud with the required stable and quiet conditions, eliminating microparticles that were suspended in an incomplete lower layer.

The manipulation runs were done at five different speeds for the exciter wire. We repeated the run at the highest speed to test for repeatability. Video recording began at time $t = 0$, when the motor drive triggered an optical gate; at this early time, the particle cloud was not yet disturbed. The wire moved 81 mm at a fixed speed in the range 50.8 to 101.6 mm/s, so that the wire required <2 s to complete its movement, including the initial acceleration and deceleration. After the wire halted, it was returned to its original position.

The response to the moving wire was the formation of a compressional pulse, which was a localized region of high density in the microparticle cloud. This compressional pulse propagated in the $+x$ direction in advance of the moving wire, as seen in the movie in the Supplemental Material [8]. Representative images are given in Fig. 2. In Fig. 2(a), the cloud was just beginning to be disturbed by the moving wire, with a compressed region forming at the left edge. A few tens of milliseconds later, in Fig. 2(b) and 2(c), the compressional pulse is seen moving from left to right. In Fig. 2(c), most microparticles that were originally in the camera's field of view had moved to the right, where they were not imaged,

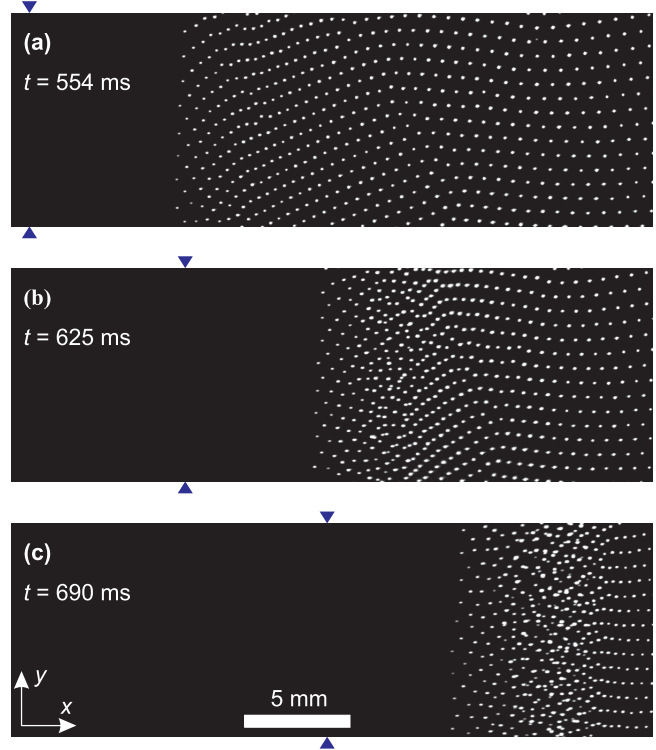


FIG. 2. Pulse evolution. A single pulse, propagating in the $+x$ direction, was excited by the movement of the wire, which is not seen because it was located above the illumination sheet; its position is marked by a pair of triangles. After the compression started in (a), a sharp leading edge developed in (b) and (c); this shape of the pulse along with its supersonic speed lead us to identify it as a shock. The undisturbed region to the right is a crystalline lattice. To the left of the pulse's peak amplitude, the areal density gradually diminishes to zero. These enhanced-contrast images have been cropped to show only the region of interest, as defined in the Supplemental Material [8], where we also present a video and raw unprocessed images. Examination of the video confirms that microparticles were displaced by the pulse only in the x direction; there was no significant bulk motion in the y direction.

but they remained confined as they were generally pushed up the far side of the bowl-shaped sheath that confined them.

IV. RESULTS

A. Identifying the pulse as a shock

The propagating compressional pulse in Fig. 2 is interpreted as a shock wave because of three observations.

(i) Our pulse's speed was supersonic. This will be demonstrated below. The Mach number for our pulse was as large as 6.2, significantly exceeding the value of 2.7 for pulses in the previous blast-wave experiments of Samsonov *et al.*, [19], where the pulse was interpreted as a shock.

(ii) Our pulse's shape has a leading edge that is much sharper than its trailing edge. This is visible in Fig. 2 and in Fig. 3 which shows profiles of a pulse's areal density.

(iii) Our pulse's amplitude was large and therefore highly nonlinear. The peak density of our pulse was ranged from 2.5

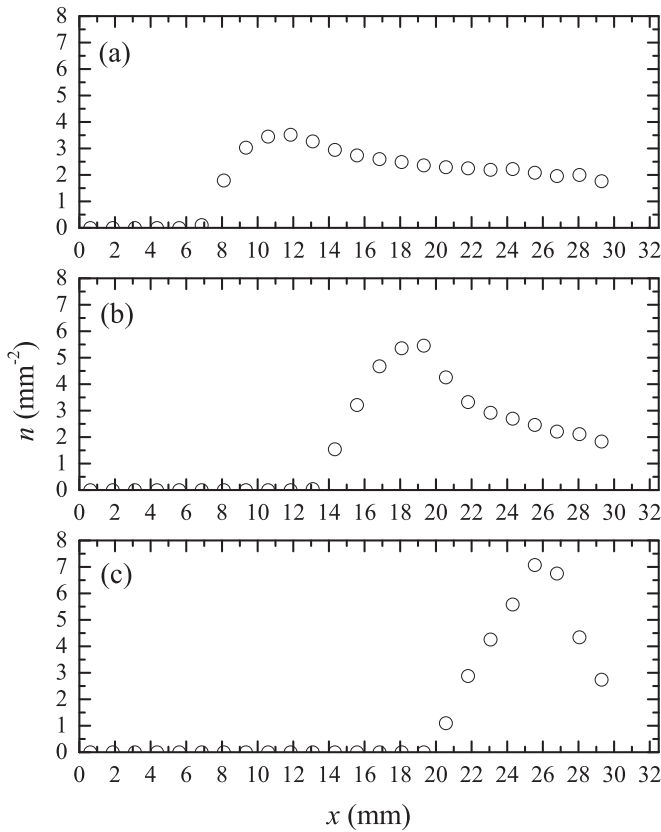


FIG. 3. Areal number density profiles. (a), (b), and (c) correspond to the respective panels of Fig. 2. The sharp leading edge of the pulse's waveform can be seen for example in (b) at $x = 20$ mm. Using plots like these, it is possible to analyze the shock waveforms' width and amplitude.

to 4.0 times the undisturbed areal density, for the six runs analyzed. The highest amplitudes corresponded to the fastest wire speeds. At such high amplitudes, the pulse must have been highly nonlinear, and to a much greater extent than in the blast-wave experiments of Samsonov *et al.* [19], where the amplitude (in what was described as a shock) was about 1.2 times the undisturbed areal density.

Based on these observations, we hereafter refer to our pulse as a shock.

B. Obtaining the shock speed

The shock's propagation speed v_{shock} was obtained as the slope in a plot of the position of the peak density vs time. Representative examples of these plots are shown in Fig. 4. Each plot included over a hundred data points, with little scatter.

As a shock propagated, the slope in Fig. 4 remained constant. Due to this constant slope, and the large number of data points, our shock speed measurements have uncertainties of only about 1%.

We attained $v_{\text{shock}} > 65$ mm/s in all our runs, as compared to the sound speed $c_l = 19.0$ mm/s. In other words, the shock's propagation was highly supersonic, with $M_{\text{shock}} > 3$.

Our highest shock speed was 117.5 mm/s, corresponding to a Mach number of $M_{\text{shock}} = 6.2$. This value, which was

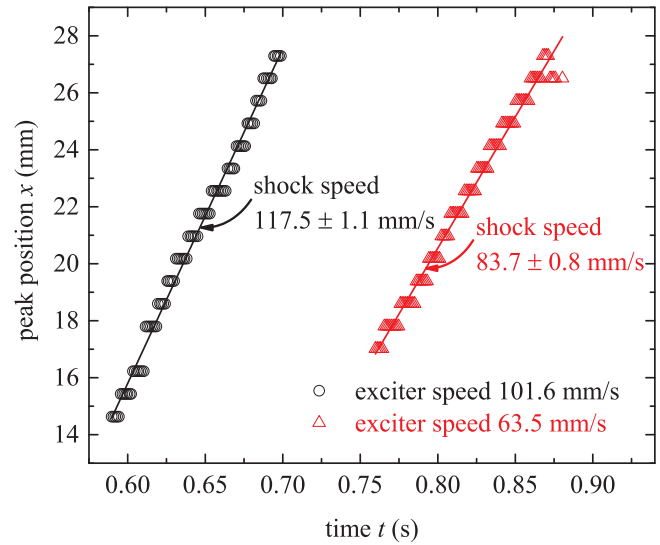


FIG. 4. Time series of the position of the pulse's peak, for two runs. The data points are the positions of peak areal density, obtained from experimental images like those in Fig. 2. Linear fits yield the shock speeds, with a small random error.

for our highest wire speed, 101.6 mm/s, was limited in our experiment only by the speed of the motor drive. As we mentioned, this Mach number significantly exceeds the result of Samsonov *et al.* [19]. In addition, it also exceeds what was attained in other previous dusty plasma shock experiments [16,17,19,22–24,29].

Our shocks are neither “weak” nor “strong,” but something in between, according to the classifications of Zel'dovich and Raizer [1]. They wrote that a shock is strong if $M_{\text{shock}} \rightarrow \infty$, and it is weak if $M_{\text{shock}} - 1 \ll 1$ [1]. The data we analyze in this paper fall in a range of $3.4 < M_{\text{shock}} < 6.2$, which is generally between the weak and strong extremes of Zel'dovich and Raizer.

C. Dependence of shock speed vs exciter speed

The main result of this paper is the dependence of the shock speed vs exciter speed, presented in Fig. 5. One run is represented by each of the six experimental data points. These data points show the value of the shock speed as obtained in Fig. 4.

To quantify the shock speed's monotonic increase with the wire speed, we present in Fig. 5 an empirical fit to the linear expression (2). This fit yielded a slope of $s = 0.98$. The value of this slope reflects the detailed character of how the medium compresses, and therefore it could be useful for, among other things, testing a theoretical equation of state for the microparticle cloud. We also note that our experimental data fit Eq. (2) well enough to say that its linear form appears to be sufficient, without requiring correction by a quadratic term.

Also shown in Fig. 5, as a dashed curve, is Eq. (4) plotted using coefficients that correspond not to the experiment, but to the simulation of Lin *et al.* [9]. We do not expect the experiment to match this curve closely,

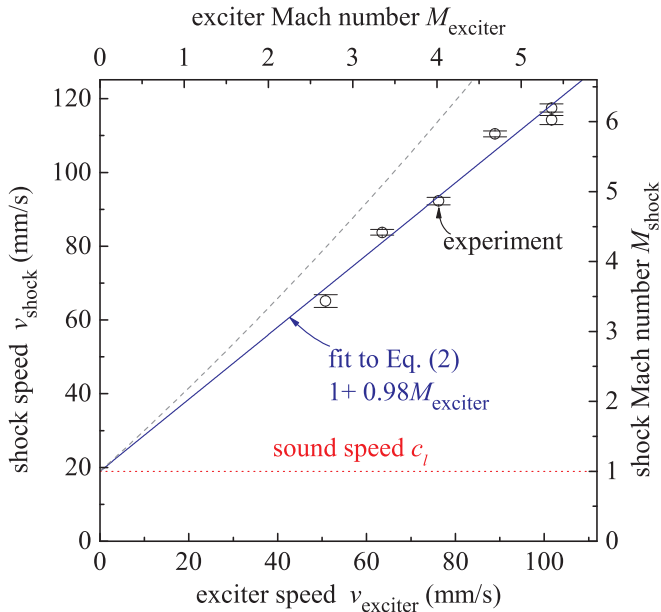


FIG. 5. Shock speed's dependence on the wire speed. The experimental data points, each representing one run, were obtained as in Fig. 4. Physical units in the left scale are normalized on the right by the sound speed, and likewise for the top scale. The error bars account for the random errors arising in the linear fits as in Fig. 4, but do not account for all sources of error, as discussed in the Supplemental Material [8]. Comparing the experimental data to empirical Eq. (2) yields $M_{\text{shock}} = 1 + 0.98M_{\text{exciter}}$. The dashed curve is Eq. (4) plotted using simulation values [9] for Γ and κ which differ from the experimental values, as explained in the text.

because the simulation was performed for parameters $\Gamma = 800$ and $\kappa = 1.5$, which are different from the

experimental values, and moreover the simulation neglected gas friction.

V. SUMMARY

We measured the dependence of the shock speed on the exciter speed in a strongly coupled 2D dusty plasma by moving an exciter wire at a constant supersonic speed. This result, in Fig. 5, was made possible by our slow sound speed and our use of particle tracking, along with our experimental advance of developing a method for continuously driving a shock. The dependence, presented in Fig. 5, allows comparing the compressional properties of our strongly coupled plasma with those of other substances, where a shock can be generated by a steadily moving piston.

Our moving exciter wire is analogous to a supersonic piston in a gas cylinder. It is also analogous to a flyer plate, which can steadily drive a planar shock for a substantial duration for the purpose of measuring equations of state [85]. Our experimental design helps meet requirements recently suggested by theorists [72] to allow comparing to models of continuously driven shocks in a strongly coupled plasma. We compared our results to a traditional empirical expression, Eq. (2), with a linear form. We also considered how our results can be compared to a quadratic form suggested in a recent simulation paper; a meaningful comparison to that expression would require additional simulations, with parameters matching our experiment, including the effects of gas drag.

ACKNOWLEDGMENTS

This work was supported by U.S. Department of Energy grant DE-SG0014566, the Army Research Office under MURI Grant W911NF-18-1-0240, and NASA-JPL subcontract 1573629.

-
- [1] Y. B. Zel'dovich and Y. P. Raizer, *Physics of Shock Waves and High-Temperature Hydrodynamic Phenomena* (Dover Publications, Mineola, NY, 2002).
 - [2] H. W. Liepmann and A. Roshko, *Elements of Gasdynamics* (Dover Publications, Mineola, NY, 2001).
 - [3] J. W. Forbes, *Shock Wave Compression of Condensed Matter* (Springer, Berlin, 2012).
 - [4] D. A. Gurnett and A. Bhattacharjee, *Introduction to Plasma Physics* (Cambridge University Press, New York, 2005).
 - [5] B. J. Alder, in *Solids under Pressure*, McGraw-Hill Series in Materials Science and Engineering, edited by W. Paul and D. M. Warschauer (McGraw-Hill, New York, 1963), Chap. 13, pp. 413–416.
 - [6] A. L. Ruoff, *J. Appl. Phys.* **38**, 4976 (1967).
 - [7] K. Nagayama, Y. Mori, K. Shimada, and M. Nakahara, *J. Appl. Phys.* **91**, 476 (2002).
 - [8] See Supplemental Material at <http://link.aps.org/supplemental/10.1103/PhysRevE.101.043211> for the apparatus, raw images and a movie for Fig. 2, cloud parameters, errors, and comments on theoretical comparison.
 - [9] W. Lin, M. S. Murillo, and Y. Feng, *Phys. Rev. E* **100**, 043203 (2019).
 - [10] V. E. Fortov, I. T. Iakubov, and A. G. Khrapak, *Physics of Strongly Coupled Plasma* (Oxford University Press, Oxford, 2006).
 - [11] M. S. Murillo, *Phys. Plasmas* **11**, 2964 (2004).
 - [12] *Strongly Coupled Coulomb Systems*, edited by G. J. Kalman, J. M. Rommel, and K. Blagoev (Springer US, Boston, MA, 2002).
 - [13] S. Cowley *et al.* (Plasma 2010 Committee), *Plasma Science: Advancing Knowledge in the National Interest* (National Academies Press, Washington, D.C., 2007).
 - [14] M. Koenig, A. Benuzzi-Mounaix, A. Ravasio, T. Vinci, N. Ozaki, S. Lepape, D. Batani, G. Huser, T. Hall, D. Hicks *et al.*, *Plasma Phys. Controlled Fusion* **47**, B441 (2005).
 - [15] G. Gregori and D. O. Gericke, *Europhys. Lett.* **83**, 15002 (2008).

- [16] D. Samsonov, J. Goree, Z. W. Ma, A. Bhattacharjee, H. M. Thomas, and G. E. Morfill, *Phys. Rev. Lett.* **83**, 3649 (1999).
- [17] A. Melzer, S. Nunomura, D. Samsonov, Z. W. Ma, and J. Goree, *Phys. Rev. E* **62**, 4162 (2000).
- [18] D. Samsonov, G. Morfill, H. Thomas, T. Hagl, H. Rothermel, V. Fortov, A. Lipaev, V. Molotkov, A. Nefedov, O. Petrov *et al.*, *Phys. Rev. E* **67**, 036404 (2003).
- [19] D. Samsonov, S. K. Zhdanov, R. A. Quinn, S. I. Popel, and G. E. Morfill, *Phys. Rev. Lett.* **92**, 255004 (2004).
- [20] V. E. Fortov, O. F. Petrov, V. I. Molotkov, M. Y. Poustylnik, V. M. Torchinsky, V. N. Naumkin, and A. G. Khrapak, *Phys. Rev. E* **71**, 036413 (2005).
- [21] J. Heinrich, S.-H. Kim, and R. L. Merlino, *Phys. Rev. Lett.* **103**, 115002 (2009).
- [22] K. Jiang, V. Nosenko, Y. F. Li, M. Schwabe, U. Konopka, A. V. Ivlev, V. E. Fortov, V. I. Molotkov, A. M. Lipaev, O. F. Petrov *et al.*, *Europhys. Lett.* **85**, 45002 (2009).
- [23] V. Nosenko and S. K. Zhdanov, *Contrib. Plasma Phys.* **49**, 191 (2009).
- [24] L. Couédel, D. Samsonov, C. Durniak, S. Zhdanov, H. M. Thomas, G. E. Morfill, and C. Arnas, *Phys. Rev. Lett.* **109**, 175001 (2012).
- [25] R. L. Merlino, J. R. Heinrich, S.-H. Kim, and J. K. Meyer, *Plasma Phys. Controlled Fusion* **54**, 124014 (2012).
- [26] Y. Saitou, Y. Nakamura, T. Kamimura, and O. Ishihara, *Phys. Rev. Lett.* **108**, 065004 (2012).
- [27] A. Usachev, A. Zobnin, O. Petrov, V. Fortov, M. H. Thoma, H. Höfner, M. Fink, A. Ivlev, and G. Morfill, *New J. Phys.* **16**, 053028 (2014).
- [28] S. Jaiswal, P. Bandyopadhyay, and A. Sen, *Phys. Plasmas* **23**, 083701 (2016).
- [29] S. K. Sharma, A. Boruah, Y. Nakamura, and H. Bailung, *Phys. Plasmas* **23**, 053702 (2016).
- [30] S. Jaiswal, M. Schwabe, A. Sen, and P. Bandyopadhyay, *Phys. Plasmas* **25**, 093703 (2018).
- [31] S. Ghosh, *Plasma Phys.* **13**, 022301 (2006).
- [32] J.-K. Xue and L.-P. Zhang, *Chaos Solitons Fractals* **32**, 592 (2007).
- [33] S. Ghosh, *JETP Lett.* **87**, 281 (2008).
- [34] S. Ghosh, *Contrib. Plasma Phys.* **48**, 569 (2008).
- [35] H. Asgari, S. V. Muniandy, and C. S. Wong, *Phys. Plasmas* **16**, 073702 (2009).
- [36] S. Ghosh, *Phys. Plasmas* **16**, 103701 (2009).
- [37] A. A. Mamun and R. A. Cairns, *Phys. Rev. E* **79**, 055401(R) (2009).
- [38] A. A. Mamun and P. K. Shukla, *New J. Phys.* **11**, 103022 (2009).
- [39] A. A. Mamun and P. K. Shukla, *Phys. Lett. A* **373**, 3161 (2009).
- [40] H. Asgari, S. V. Muniandy, and C. S. Wong, *Plasma Phys.* **18**, 013702 (2011).
- [41] G. C. Das, B. Choudhury, and M. P. Bora, *Phys. Plasmas* **19**, 044502 (2012).
- [42] H. Asgari, S. V. Muniandy, and C. S. Wong, *Plasma Phys.* **20**, 013704 (2013).
- [43] Y. Wang, X. Guo, Y. Lu, and X. Wang, *Phys. Lett.* **380**, 215 (2016).
- [44] A. N. Dev and M. K. Deka, *Braz. J. Phys.* **47**, 532 (2017).
- [45] H. Charan and R. Ganesh, *Phys. Plasmas* **25**, 043706 (2018).
- [46] F. Li and O. Havnes, *Phys. Rev. E* **64**, 066407 (2001).
- [47] P. M. Bellan, *Fundamentals Of Plasma Physics* (Cambridge University Press, Cambridge, 2008).
- [48] A. Piel, *Plasma Physics* (Springer, Berlin, 2010).
- [49] V. Fortov, I. Iakubov, and A. Khrapak, *Physics of Strongly Coupled Plasma* (Oxford University Press, Oxford, 2007).
- [50] P. K. Shukla and A. A. Mamun, *Introduction to Dusty Plasma Physics*, Series in Plasma Physics (Institute of Physics Publishing, Bristol, 2001).
- [51] V. N. Tsytovich, G. E. Morfill, S. V. Vladimirov, and H. M. Thomas, *Elementary Physics of Complex Plasmas*, Vol. 731 of Lecture Notes in Physics (Springer, Berlin, 2008).
- [52] S. V. Vladimirov, *Physics and Applications of Complex Plasmas* (Imperial College Press, London, 2005).
- [53] A. Melzer, *Physics of Dusty Plasmas*, Vol. 962 of Lecture Notes in Physics (Springer International Publishing, Cham, 2019).
- [54] I. H. Hutchinson, *Plasma Phys. Controlled Fusion* **47**, 71 (2004).
- [55] Tech. Rep., U.S. Department of Energy. Office of Science (2016), URL https://science.osti.gov/-/media/fes/pdf/program-news/Frontiers_of_Plasma_Science_Final_Report.pdf.
- [56] J. Goree, *Low Temperature Plasmas: Fundamentals, Technologies and Techniques* (Wiley-VCH, Berlin, 2008), Chap. 6, pp. 157–206.
- [57] A. V. Ivlev, U. Konopka, G. Morfill, and G. Joyce, *Phys. Rev. E* **68**, 026405 (2003).
- [58] C. A. Knaepk, D. Samsonov, S. Zhdanov, U. Konopka, and G. E. Morfill, *Phys. Rev. Lett.* **98**, 015004 (2007).
- [59] P. Hartmann, A. Douglass, J. C. Reyes, L. S. Matthews, T. W. Hyde, A. Kovács, and Z. Donkó, *Phys. Rev. Lett.* **105**, 115004 (2010).
- [60] Y. Feng, J. Goree, and B. Liu, *Phys. Rev. Lett.* **104**, 165003 (2010).
- [61] Y. Feng, J. Goree, and B. Liu, *Phys. Rev. E* **82**, 036403 (2010).
- [62] V. Nosenko, S. K. Zhdanov, A. V. Ivlev, C. A. Knaepk, and G. E. Morfill, *Phys. Rev. Lett.* **103**, 015001 (2009).
- [63] E. A. Kononov, M. M. Vasiliev, and O. F. Petrov, *J. Exp. Theor. Phys.* **126**, 600 (2018).
- [64] L.-J. Hou, Z. L. Mišković, A. Piel, and M. S. Murillo, *Phys. Rev. E* **79**, 046412 (2009).
- [65] W. Li, D. Huang, K. Wang, C. Reichhardt, C. J. O. Reichhardt, M. S. Murillo, and Y. Feng, *Phys. Rev. E* **98**, 063203 (2018).
- [66] M. S. Murillo and D. O. Gericke, *J. Phys. A* **36**, 6273 (2003).
- [67] V. A. Schweigert, V. M. Bedanov, I. V. Schweigert, A. Melzer, A. Homann, and A. Piel, *J. Exp. Theor. Phys.* **88**, 482 (1999).
- [68] O. Arp, D. Block, A. Piel, and A. Melzer, *Phys. Rev. Lett.* **93**, 165004 (2004).
- [69] J. K. Meyer and R. L. Merlino, *Phys. Plasmas* **20**, 074501 (2013).
- [70] R. Fitzpatrick, *Theoretical Fluid Mechanics* (IOP Publishing, Bristol, 2017).
- [71] S. K. Tiwari and A. Sen, *Phys. Plasmas* **23**, 100705 (2016).
- [72] M. Marciantie and M. S. Murillo, *Phys. Rev. Lett.* **118**, 025001 (2017).
- [73] Y. Feng, J. Goree, and B. Liu, *Rev. Sci. Instrum.* **78**, 053704 (2007).

- [74] Y. Feng, J. Goree, and B. Liu, *Rev. Sci. Instrum.* **82**, 053707 (2011).
- [75] Y. Feng, J. Goree, Z. Haralson, C.-S. Wong, A. Kananovich, and W. Li, *J. Plasma Phys.* **82**, 615820303 (2016).
- [76] A. Melzer, M. Himpel, H. Krüger, M. Mulsow, and S. Schütt, *Plasma Phys. Controlled Fusion* **61**, 014029 (2018).
- [77] C. Durniak and D. Samsonov, *Europhys. Lett.* **90**, 45002 (2010).
- [78] C. Durniak and D. Samsonov, *Phys. Rev. Lett.* **106**, 175001 (2011).
- [79] P. Hartmann, A. Z. Kovács, A. M. Douglass, J. C. Reyes, L. S. Matthews, and T. W. Hyde, *Phys. Rev. Lett.* **113**, 025002 (2014).
- [80] L.-W. Teng, P.-S. Tu, and L. I., *Phys. Rev. Lett.* **90**, 245004 (2003).
- [81] C.-L. Chan, W.-Y. Woon, and L. I., *Phys. Rev. Lett.* **93**, 220602 (2004).
- [82] J. Carstensen, F. Greiner, and A. Piel, in *Dusty/Complex Plasmas: Basic and Interdisciplinary Research: Sixth International Conference on the Physics of Dusty Plasmas*, edited by V. Yu. Nosenko, P. K. Shukla, M. H. Thoma, and H. M. Thomas, AIP Proc. Conf. No. 1397 (AIP, New York, 2011).
- [83] C. A. Schneider, W. S. Rasband, and K. W. Eliceiri, *Nat. Methods* **9**, 671 (2012).
- [84] S. Nunomura, J. Goree, S. Hu, X. Wang, and A. Bhattacharjee, *Phys. Rev. E* **65**, 066402 (2002).
- [85] M. D. Knudson, D. L. Hanson, J. E. Bailey, C. A. Hall, J. R. Asay, and W. W. Anderson, *Phys. Rev. Lett.* **87**, 225501 (2001).